20. Polyadenylated RNA's were prepared (*21*) from piglet testes (10 to 20 days old). Random-primed cDNA synthesis, size selection (0.5 to 2 kb), and cloning into λgt11 vector were as described (*22*). The expression library (3×10^6 clones) was screened (*23*) with a mixture of ten monoclonal antibodies to the porcine LH-hCG receptor (*3*). Three positive clones that cross-hybridized were selected (pLHR 1 to 3) and sequenced. The longer insert (a 1-kb Eco RI fragment from pLHR1) was ^{32}P-labeled by random priming and was used to probe 2×10^6 clones from a second size-selected (2 to 6 kb) cDNA library in λgt10 vector. Six overlapping clones from the 400 detected signals (selected for length) were used for sequencing (*24*).
21. H. Loosfelt, F. Logeat, M. T. Vu Hai, E. Milgrom, *J. Biol. Chem.* **259**, 14196 (1984).
22. H. Loosfelt *et al.*, *Proc. Natl. Acad. Sci. U.S.A.* **83**, 9045 (1986).
23. T. V. Huynh, R. A. Young, R. W. Davis, in *DNA Cloning: A Practical Approach*, D. M. Glover, Ed. (IRL, Oxford, 1985), vol. 1, p. 98.
24. M. Misrahi *et al.*, *Biochem. Biophys. Res. Commun.* **143**, 740 (1987).
25. The full-length open reading frame of the receptor (nucleotides −11 to 2113, see sequence in Fig. 2) was inserted into the Bgl II site of the pKSV10 vector (Pharmacia). COS-7 cells were grown and transfected (*26*) with 10 μg of vector DNA per 10^6 cells. After 42 hours of transient expression, cell membranes were isolated (*27*). Radioligand binding assays were carried out in duplicate: membranes (1.5 mg of protein per milliliter) were incubated in 0.4 ml of phosphate-buffered saline containing 0.1% sodium azide and various amounts of ^{125}I-labeled hCG (0.5 μCi/pmol), for 12 hours at 37°C. The mixture was centrifuged at 10,000*g* and the pellets were washed once with 1 ml of buffer; bound radioactivity was then measured. The nonspecific binding was determined by parallel incubations with unlabeled $2.10^{-7}M$ hCG and this amount was subtracted from total binding.
26. A. Guiochon-Mantel *et al.*, *Nature* **336**, 695 (1988).
27. V. Rebois, *J. Cell. Biol.* **94**, 70 (1982).
28. We thank P. Dessen for help in computer analysis and D. Grebert for technical assistance.

23 May 1989; accepted 23 June 1989

Domain Separation in the Activation of Glycogen Phosphorylase *a*

E. J. GOLDSMITH, S. R. SPRANG, R. HAMLIN, N.-H. XUONG, R. J. FLETTERICK

The crystal structure of glycogen phosphorylase *a* complexed with its substrates, orthophosphate and maltopentaose, has been determined and refined at a resolution of 2.8 angstroms. With oligosaccaride bound at the glycogen storage site, the phosphate ion binds at the catalytic site and causes the regulatory and catalytic domains to separate with the loss of stabilizing interactions between them. Homotropic cooperativity between the active sites of the allosteric dimer results from rearrangements in isologous contacts between symmetry-related helices in the subunit interface. The conformational changes in the core of the interface are correlated with those observed on covalent activation by phosphorylation at Ser^{14} (phosphorylase *b* → *a*).

GLYCOGEN PHOSPHORYLASE (GP) (E.C. 4.2.1.1) is a cooperative homodimer that catalyzes the degradative phosphorolysis of glycogen. The enzyme is regulated by covalent phosphorylation (*1*) and by substrates and effectors (*2*). The substrates phosphate, glucose-1-phosphate (G1P), and glycogen bind cooperatively (*3*) and, in terms of the two-state model (*4*), drive the conformational equilibrium from the catalytically inactive T-state to the active R-state conformation. Of special interest are the conformational changes required to bind these substrates and the mechanisms by which the allosteric effectors promote these changes. Comparison of the high-resolution crystal structures of the dephosphorylated (GP*b*) and phosphorylated (GP*a*) enzymes (*5*), the latter under glucose inhibition, has shown that phosphorylation of Ser^{14} results in the formation of extensive subunit contacts on the regulatory face of the molecule. Similar changes are induced by the activator adenosine monophosphate (AMP) (*6*). However, the active-site–bound glucose in GP*a* crystals blocks structural changes at the catalytic site that might otherwise occur in the free enzyme on phosphorylation. Previous attempts to grow crystals of GP*a* with substrates bound or in the absence of glucose have been unsuccessful. Madsen *et al.* (*7*) found that fresh crystals of GP*a* tend to disintegrate when exposed to a combination of AMP, oligosaccharide, and G1P, although such crystals can reanneal to form a stable lattice with expanded unit cell dimensions. In contrast, crystals of GP*a* that have become naturally cross-linked while aging maintain their integrity in the presence of substrates and activators and diffract to moderate resolution.

To probe the active conformation of phosphorylase *a*, we substituted glucose in crystals of GP*a* with orthophosphate and maltopentaose by diffusion. The refined 2.8 Å resolution structure contains phosphate ion bound in the catalytic site and maltopentaose bound only in the storage-activation site. Together, the two substrates induce local conformational changes in the catalytic site and a domain separation, as well as rearrangements at the subunit interface that are not observed when either alone is present (*8, 9*). However, natural cross-linking and lattice forces may restrain the enzyme from undergoing a complete transition to the R state.

After diffusion of the substrates orthophosphate and maltopentaose into crystals of GP*a*, the volume of the tetragonal unit cell (Table 1) increases by 28,100 Å (*3*), primarily as a result of a 1.7 Å expansion along the crystallographic *c*-axis, and the resolution of observable diffraction decreases from 2.0 to 2.8 Å (*10*). Diffraction data were measured on the Mark II multiwire area detector (*11*). Crystals containing orthophosphate and maltopentaose show substantial nonisomorphism with respect to the parent crystals, with an average change of 43% in structure-factor amplitudes (*8*). The structure was determined by a sequence of rigid body and restrained group

Table 1. Crystal data and refinement parameters for substrate-inhibited GP*a* (space group $P4_32_12$). For comparison, data are also shown for glucose-inhibited GP*a*. The scaling *R*-factor between data sets is 0.36; $R_{sym} = \{\Sigma_{hkl}\Sigma_n[(I^n_{hkl} - I_{hkl})/I_{hkl}]\}/N_{hkl}$, where I^n_{hkl} is the *n*th measurement of I_{hkl}; $R_{cryst} = \Sigma_{hkl}\ [||F(obs)_{hkl}| - |F(calc)_{hkl}||]/|F(obs)_{hkl}|$, where $|F(obs)|$ and $|F(calc)|$ are the observed and calculated structure factor amplitudes, respectively.

Parameter	GP*a*	
	Activated	Inhibited
	Crystal data	
Unit cell dimensions		
a (Å)	128.5	128.4
c (Å)	118.1	116.4
Resolution (Å)	2.8	2.1
Reflections	23,035	35,231
R_{sym}	0.06	0.05
	Refinement parameters	
Protein atoms	6695	6624
Δ bond* (Å)	0.013	0.015
Δ angle* (Å)	0.050	0.050
Resolution (Å)	50 to 2.8	50 to 2.1
Reflections	21,753	34,792
R_{cryst}	0.19	0.16

*Applied restraints were 0.01 Å on bonds and 0.03 Å on angles.

E. J. Goldsmith, Department of Biochemistry, University of Texas Southwestern Medical Center, Dallas, TX 75235.
S. R. Sprang, Howard Hughes Medical Institute, University of Texas Southwestern Medical Center, Dallas, TX 75235.
R. Hamlin and N.-H. Xuong, Departments of Physics, University of California San Diego, La Jolla, CA 92093.
R. J. Fletterick, Department of Biochemistry and Biophysics, University of California San Francisco, San Francisco, CA 94143.

crystallographic refinement, in which the atomic coordinates of the glucose-inhibited parent structure were used as an initial model (*12*), followed by map interpretation and conventional restrained refinement (*13*) to a final crystallographic *R*-factor of 0.187 (Table 1). The root-mean-square (rms) displacements of atomic coordinates from the parent structure (after least-squares superposition of the dimers) is 0.83 Å for backbone Cα atoms (Table 2) and 1.2 Å for all atoms, significantly greater than the estimated upper bound for the error in coordinates of 0.28 Å (*14*). The shifts in side chain and main chain positions reported below represent correlated changes in atomic positions and are readily visible as changes in the electron density.

In the activated structure, the catalytic site (Figs. 1 and 2) contains a phosphate ion bound between the reverse β-turn active-site gate (282 to 285; "G" in Fig. 1B) and the amino terminus of the active-site helix (133 to 150), forming hydrogen bonds with the peptide amide groups of Gly^{135} and Leu^{136}. In contrast to the heptenitol phosphate–GP*b* complex reported by McLaughlin *et al.* (*15*), the orthophosphate is well outside (7.7 Å P–P distance) of van der Waals contact distance of the coenzyme pyridoxal phosphate (PLP) phosphate group. A phosphate ion is also observed at the nucleotide activator site. Two molecules of maltopentaose bind at the glycogen storage activation domain (*8*), but no oligosaccharide is observed at the catalytic site.

The largest conformational change occurs in the catalytic site where the phosphate ion

Table 2. Root-mean-square differences in Cα positions between activated and glucose-inhibited GP*a*. Coordinates of Cα atoms of the glucose-inhibited GP*a* dimer were superimposed by least squares (*21*) onto the corresponding Cα coordinates of activated GP*a*, entry 5-838(D). The glucose-inhibited GP*a* coordinates thus transformed served as the basis set for the subsequent superpositions.

Residue range	Difference, rms (Å)	Translation (Å)			Rotation (degrees)		
		Δx	Δy	Δz	φ	ϕ	χ
5–838(D)	0.83	0.65	0.34	0.90	−1.5	45	0.2
5–838	0.48	0.08	−0.80	−0.17	21	89	1.0
5–486	0.48	−0.54	−0.64	0.07	17	99	1.0
160–278	0.56	−0.13	−0.71	0.03	10	95	1.0
486–838	0.43	0.27	−0.89	0.27	33	86	1.3

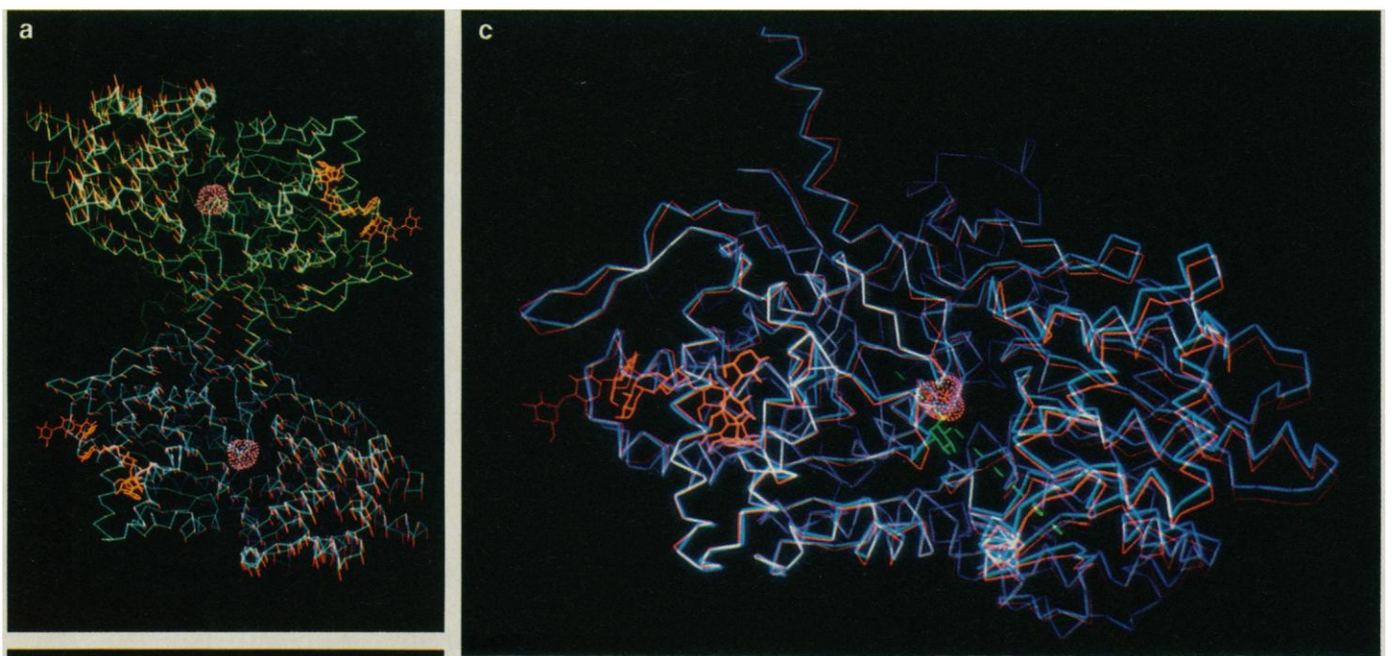

Fig. 1. Glycogen phosphorylase is a dimer of identical 842–amino acid subunits. Each subunit is composed of two major domains. The amino terminal or "regulatory" domain consists of the first 486 residues and 813 to 842; it contains all of the regulatory sites and residues that form the subunit interface. The carboxyl terminal or "catalytic" domain consists of residues 487 to 812 and contains the pyridoxal phosphate cofactor (PLP680). (**a**) Backbone Cα diagram of glucose-inhibited GP*a* dimer. Subunits are colored cyan and green. The active-site–bound phosphate in activated GP*a* is represented by a magenta van der Waals surface; two chains of maltopentaose at storage site are shown in red. Red shift vectors represent translations in Cα positions from the parent (glucose-inhibited) to the substrate-activated structure; vectors were calculated from superimposed dimers, averaged over ten residues, and magnified by 2.5. The view is shown along the diad axis looking into the catalytic sites of the subunits, the phosphorylation and nucleotide effector sites are behind. (**b**) Schematic of monomer (drawn using RIBBON by M. W. Carson and H. N. McNutt). All ligands are shown in white: inorganic phosphate at the active site is bound behind the active-site gate (residues 282 to 285) and at the amino terminus of the active-site helix, and the phosphate bound to the AMP site is visible on the regulatory face (at the back in this view). The amino-terminal domain is red except that the tower helix "T" (261 to 278), active-site gate "G" (280 to 286), and α8 (287 to 314) helix (unlabeled) are white, and the central interface β strand (185 to 194), adjoining Dali loop "D" (162 to 184), and top loop "TL" (196 to 220) are yellow; the carboxyl-terminal domain is blue (561 to 812), and the polypeptide chains connecting the domains and adjoining structures (442 to 561) are green. The active-site helix and glycine-rich loop (130 to 132) are red and located directly behind the phosphate ion and the gate. The subunit interface consists of the NH_2-terminus (1 to 120), central interface β strand (185 to 194), and the tower helix. (**c**) Superposition of substrate-activated (red) and glucose-inhibited (cyan) GP*a* subunits. The Cα positions of residues 5 to 280 of the dimer were used in the superposition; the approximate path of the domain rotation axis is shown as a green dashed line.

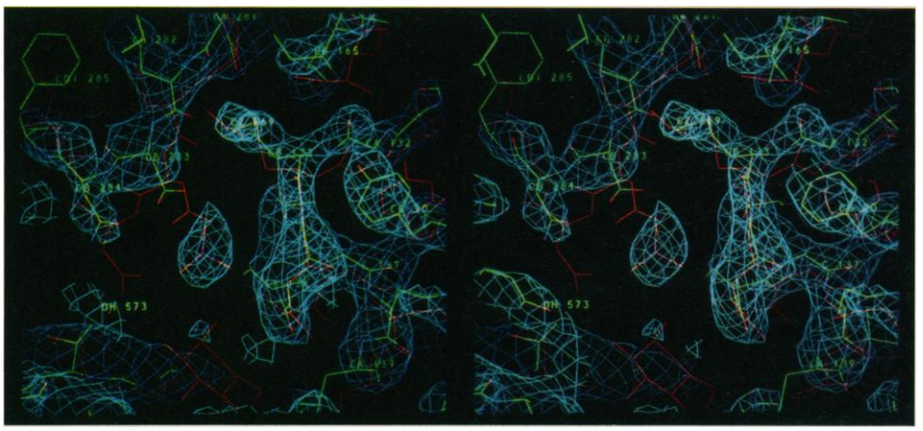

Fig. 2. The $2F_o - F_c$ Fourier map of substrate-activated GP*a* contured at 0.15 e/Å^3 in the region of the catalytic site. The atomic model of the activated structure and the phosphate group are colored by atom, C, green; N, blue; O, red, and P, magenta. The glucose-inhibited structure, including glucose, is shown in red. Note the displacement of the active-site gate (282 to 285), the 30° rotation about the Tyr^{90} Cα–Cβ bond, and rotation of the carbonyl oxygen of Gly^{137} away from the helix axis to form a hydrogen bond with Phe^{141} N.

displaces Asp^{283} and the active-site gate (Fig. 2). This rearrangement, which has been observed in other phosphorylase-substrate complexes (*9, 16*), occurs because the phosphate ion and the Asp^{283} carboxylate occupy overlapping sites. The conformational mobility of residues 282 to 286 increases markedly, and the side chains of Asp^{283} and Phe^{285} are almost completely disordered. As the gate moves away from the active site, the hydrogen bond between Pro^{281} of the gate and Arg^{569} is broken. The second major conformational change induced by phosphate binding occurs in the main chain of residues Gly^{130} to Gly^{132} in the loop preceding the active-site helix (see below).

The rearrangement of the active-site gate reveals the structural basis for the negative cooperativity observed between purines and substrates (*17*). Purines and purine nucleosides stabilize the T-state conformation by intercalating between the aromatic side chains of Phe^{285} and Tyr^{613} at the domain interface. Displacement of the active-site gate by phosphate disorders Phe^{285} and the purine effector site is destroyed.

The perturbations at the catalytic and glycogen-binding sites trigger rearrangements at the subunit interface and reorientation of the catalytic (residues 486 to 842) and regulatory (1 to 485) domains of the subunits (Table 2). In the subunit interface, the β strands (184 to 195), which form the core of the interface and peptide extensions (162 to 183 and 196 to 220; "D" and "TL" in Fig. 1B) together with the tower helices (residues 260 to 280; "T" in Fig. 1B), rotate 1° toward the corresponding residues in the opposite subunit. The axis of this rotation is approximately parallel with the molecular diad axis and is nearly colinear with the α8 helix (287 to 314, Fig. 1B).

In each subunit, the catalytic domain rotates 1.3° and is translated by 0.95 Å away from the regulatory domain and the subunit interface (Fig. 1C and Table 2), thereby opening the active-site crevice. The domain rotation axis passes between the domains at the rear of the catalytic site and intersects the midpoints of both the active-site helix and the α2 helix in the amino terminal interface segment (Fig. 1C), which undergo conformational changes on AMP (*6*) activation. Residues furthest from the rotation axis shift (with respect to Cα positions) by 1.6 Å. Together, the domain and subunit rearrangements increase the accessibility of the active site. Overall, a net loss of hydrogen bonds between the catalytic and regulatory domains occurs within the active site and elsewhere in the domain interface.

The global character of both the quaternary and domain movements is evident in the change in distance between residues related by the diad axis of the phosphorylase dimer (Fig. 3). Residues in the catalytic domain (486 to 812) move away from the diad axis. The motion is more complex in the regulatory domain, and elements of the subunit interface (190 to 195 and 261 to 274) move toward their counterparts in the opposite subunit. These rearrangements are accompanied by numerous changes in hydrogen bonds and van der Waals interactions throughout the molecule.

The catalytic sites of opposite subunits communicate through changes in the isologous contacts between the tower helices and central interface β strands (Figs. 1A and 4). The active-site gate displaced by phosphate binding is covalently linked to the tower helix and to the tower helix of the opposite subunit through van der Waals contacts (Figs. 4 and 5). On substrate activation, the tower helices move toward each other laterally (Fig. 1A and 4), decreasing the distance between their axes by 2.0 Å in the plane of Asn^{270}. The more intimate "ridge into groove" (*18*) interactions between the tower helices in the activated structure are accommodated by local unwinding of the helix with the loss of a main chain hydrogen bond between Asn^{270} and Asn^{274}. The length of the helix increases by approximately 1.4 Å from Tyr^{262} to Val^{278}. The hydrogen bonds between the tower helices, although altered in stereochemistry, remain largely intact in the activated dimer. The van der Waals contact between Pro^{281} and Tyr$^{262'}$ of the diad-related subunit, which is maintained in both structures, couples the movement in the active-site gate to the tower helices.

The conformational changes in residues Gly^{130} to Gly^{132} near the phosphate binding site also link the active site with the subunit interface (Figs. 2 and 5). In the parent structure, Gly^{130} is in van der Waals contact with Tyr^{90}. In the activated enzyme, rotations about main chain bonds in residues 129 to 132 cause Gly^{130} to lose contact with Tyr^{90} and form a new stacking interaction with the aromatic side chain of Trp^{182}. The

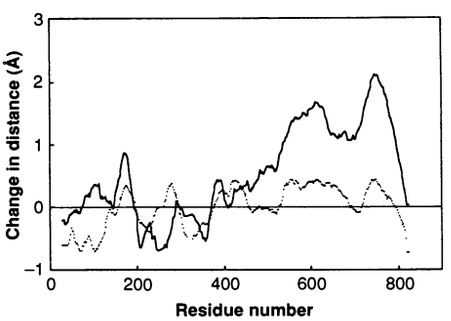

Fig. 3. Change in distance between residues related by the diad axis of symmetry of the dimer, averaged over a 35-residue window. Solid line, activated GP*a* − GP*a*. The carboxy terminal catalytic domains show dramatic separation from the diad axis on substrate activation. The function changes sign where the polypeptide passes the twofold axis, at residues 54, 190, and 273: the centers of the three interface segments. The carboxyl-terminal segment (residues 810 to 842) moves in concert with the regulatory domain with which it forms its most extensive contact surface. The "Dali" loop (residues 162 to 182, Fig. 1B) forms extensive contacts with the catalytic domain and moves away from the subunit interface on activation. Approximately 130 hydrogen bonds present in either the parent or activated structure change in contact distance by more than 1 Å and 50 of these by more than 2 Å. Dotted lines, GP*a* − GP*b*. The 115 amino-terminal residues and those in the central interface and top loop (193 to 220) approach each of their counterparts in the opposite subunit. The correlation coefficient computed for the two vector shift sets at corresponding positions, averaged over a 35-residue window (as shown), is 0.61.

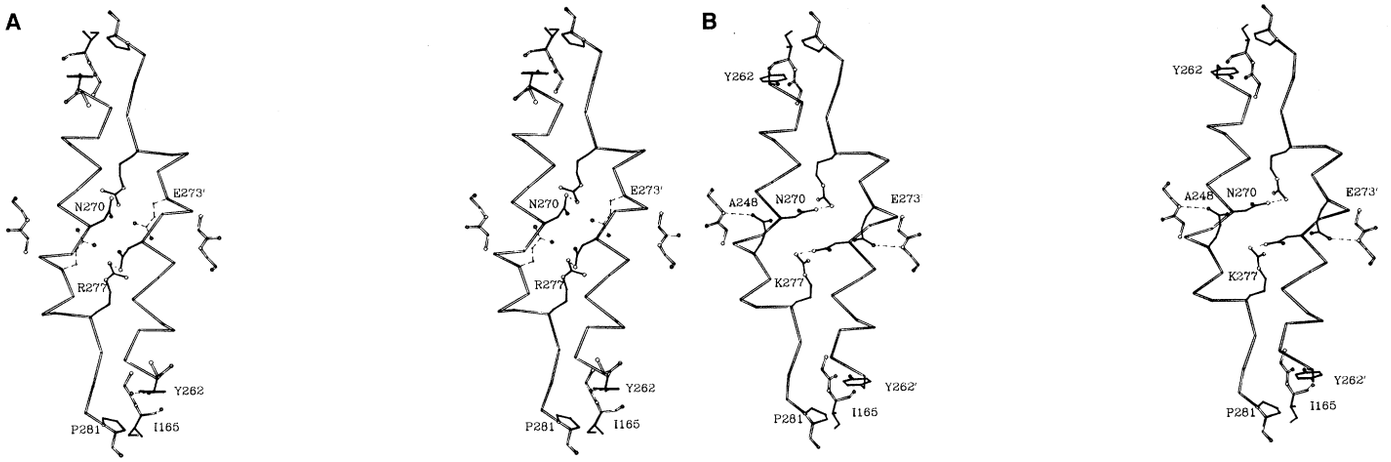

Fig. 4. Tower helices (262 to 281) in the subunit interface. (**A**) Glucose-inhibited GP*a* and (**B**) activated GP*a*. The major interaction changes involve Asn^{270}, Glu^{273}, and Arg^{277}, which face the solvent-filled cavity at the core of the subunit interface. The side chain of Glu^{273} is disordered in the activated crystals (dashed lines) and loses contact with the neighboring β strand (A248). A large rotation is also observed on a solvent-accessible leucine, Leu^{271} (not shown). Tyr^{262} of tower helix forms contacts with the active-site gate of the opposite subunit.

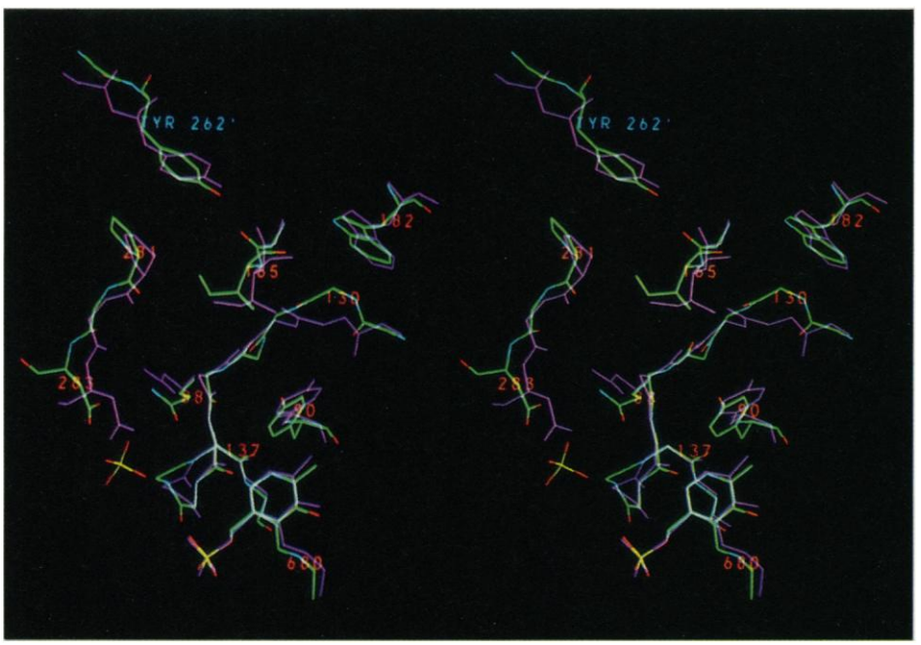

Fig. 5. The linkage between conformational changes in the active site, glycine-rich loop, and Tyr^{90}, with the subunit interface and domain interface (see text). Superpositions of activated GP*a* (colored by atom as in Fig. 2) with glucose-inhibited GP*a* (magenta). A new hydrogen bond (Glu^{88} Oε1 : Gly^{137} N) appears in the activated structure.

main chain hydrogen bond that stabilizes a single turn of helix between residues 183 to 186 is consequently broken (not shown), affecting the conformation of Tyr^{185} in the central interface β strand. Two residues, Tyr^{185} and Pro$^{194'}$ that form the contact between β strands in symmetry-related subunits, slide past each other, resulting in a relative motion of ~1 Å between subunits. The change in orientation of Gly^{132} is propagated to the subunit interface through contacts with Leu^{165} and Gly^{164} to Tyr$^{262'}$ (Fig. 5). Tyr^{90} rotates to form a new stacking interaction with the peptide bond of residue 132 but maintains van der Waals contact with the pyridoxal ring of the cofactor in the catalytic domain that is also present in the glucose-inhibited enzyme (Fig. 5).

The structural transitions induced by covalent phosphorylation are correlated with those promoted by substrate binding. As is apparent in the change in distance between diad-related residues (Fig. 3), both transitions promote subunit interactions. In the presence of the active-site–bound inhibitor glucose, phosphorylation increases the number of interactions between subunits involving residues near the phosphorylation and AMP binding sites in the amino terminus (residues 5 to 120). Release of the enzyme from glucose inhibition and substrate activation results in the formation of additional intersubunit contacts involving the remainder of the interface (residues 160 to 220 and 260 to 280). These changes are coupled to domain separation. The conformational changes induced by covalent phosphorylation and those promoted by substrate binding appear to be separable steps in the activation pathway.

The catalytic site of phosphorylase is situated at the domain interface, much as in dimeric "hinge" proteins hexokinase, citrate synthase, and aspartate aminotransferase (*19*). Homotropic cooperativity occurs because domain rotation is coupled to changes in the isologous contacts between subunits. In contrast, the active sites of the allosteric enzymes phosphofructokinase and aspartate carbamoyl transferase (*20*) are located in the subunit interface, and cooperative substrate binding is modulated mainly by subunit rotations.

Phosphorylase is the only enzyme known for which effector-substrate binding induces an "open" conformation, in which domains separate, rather than a "closed" conformation, in which the domains move together. The rotational component of the domain separation observed in substrate-activated phosphorylase crystals is small (1.3°) in contrast to the 4° to 12° rotations observed in other hinge proteins (*19, 20*). Since we have analyzed crystals in which substrate activation is limited by lattice forces, it could be expected that the complete T → R transition involves larger structural changes.

REFERENCES AND NOTES

1. E. G. Krebs and E. H. Fischer, *J. Biol. Chem.* **212**,

121 (1956).
2. D. J. Graves and J. H. Wang, *Enzymes* 7, 435 (1972); R. J. Fletterick and N. B. Madsen, *Annu. Rev. Biochem.* **245**, 31 (1980).
3. A. D. Engers, S. Schechosky, N. B. Madsen, *Can. J. Biochem.* **48**, 746 (1970); A. M. Gold, R. M. Johnson, J. K. Tseng, *J. Biol. Chem.* **245** (1970); P. J. Kasvinsky, N. B. Madsen, R. J. Fletterick, J. Syguch, *ibid.* **253**, 1290 (1978).
4. J. Monod, J. Wyman, J. P. Changeux, *J. Mol. Biol.* **12**, 88 (1965).
5. S. R. Sprang *et al.*, *Nature* **336**, 215 (1988).
6. S. Sprang, E. Goldsmith, R. Fletterick, *Science* **237**, 1012 (1987).
7. N. B. Madsen, P. J. Kasvinsky, R. J. Fletterick, *J. Biol. Chem.* **253**, 9097 (1978). Parent crystals of phosphorylase *a* contained the T-state effector glucose [E. Helmreich, M. C. Michaelides, C. F. Cori, *Biochemistry* **6**, 3695 (1967)] bound at the catalytic site. Crystals were equilibrated in glucose-free storage buffer [10 m*M* 2-[bis(2-hydroxyethyl)amino]ethane sulfonic acid (Bes), 10 m*M* $MgCl_2$, *p*H 6.8] and then soaked for 4 to 8 hours in the same buffer containing 0.1*M* KH_2PO_4 and 0.3*M* maltopentaose (Boehringer Mannheim). Aged crystals did not redissolve in the glycerol phosphate buffer used to assay. However, crushed crystals incorporate about 10% as much ^{14}C from glucose-1-phosphate into maltopentaose as the phosphorylase *a* from Boehringer measured in a 30-min reaction time [determined by the method of M. Kobayashi, G. Soman, D. J. Graves, *J. Biol. Chem.* **257**, 14041 (1982)].
8. The average $|\Delta F|/|F| = 0.43$, where $\Delta F = F_{gp} - F_{par}$, compared with 0.082 for maltopentaose alone [E. Goldsmith, S. Sprang, R. J. Fletterick, *J. Mol. Biol.* **156**, 411 (1982); E. J. Goldsmith and R. J. Fletterick, *J. Pure Appl. Chem.* **55**, 577 (1983)]. Maltopentaose alone induced global changes that are highly correlated with but much reduced in magnitude (25%) from the changes induced by both ligands and caused virtually none of the specific changes induced by phosphate in active site.
9. S. G. Withers, N. B. Madsen, S. R. Sprang, R. J. Fletterick, *Biochemistry* **21**, 5372 (1982).
10. Mosaicity of the crystals increases, as indicated by the change in peak width at half the height of the 008 reflection, from 0.11° in the parent crystals to 0.22° in activated crystals.
11. N.-H. Xuong, S. T. Freer, R. Hamlin, C. Nielson, W. Vernon, *Acta Cryst.* **A34**, 289 (1978).
12. S. R. Sprang *et al.*, unpublished results.
13. The position of the subunit in the unit cell of the activated crystals was refined by using the rigid body least-squares refinement program CORELS [J. L. Sussman, S. R. Holbrook, G. M. Church, S. H. Kim, *Acta Cryst.* **A33**, 800 (1977)] using the 1500 strongest reflections to 4.5 Å, evenly distributed in reciprocal space. Restrained crystallographic refinement using an FFT version of PROLSQ [W. A. Hendrickson and J. Konnert, in *Biomolecular Structure, Function, Conformation and Evolution*, R. Srinivasan, Ed. (Pergamon, London, 1981), vol. 1, pp 43–47]; incorporated restraints to the phi and psi angles of residues in 55 segments, each corresponding to single elements of α-helical or β-strand secondary structure. After 30 cycles, data to 3.4 Å resolution were included and the torsional restraints were relaxed. Cycles 52 to 101 were carried out with all data to 2.8 Å resolution. The model was rebuilt into electron density maps calculated with coefficients $(2|F_o| - |F_c|)$ using the molecular modeling program FRODO [T. A. Jones, *Acta Cryst.* **11**, 268 (1978)]. Temperature factor refinement was initiated after cycle 78. Cycles 102 to 124 were carried out with the TNT package [D. E. Tronrud, L. F. TenEyck, B. W. Matthews, *Acta Cryst.* **A43**, 489 (1987)] to include the solvent contribution to the structure factors. The solvent was modeled as a continuum of electron density scaled at 0.3 e/Å^3 and solvent $B = 70$ Å^2. No attempt was made to locate ordered water molecules.
14. P. V. Luzzati, *Acta Cryst.* **5**, 802 (1952).
15. P. J. McLaughlin, D. I. Stuart, H. W. Klein, N. G. Oikonomakos, L. N. Johnson, *Biochemistry* **23**, 5862 (1984).
16. J. Hadju *et al.*, *EMBO J.* **6**, 539 (1987).
17. S. R. Sprang *et al.*, *Biochemistry* **21**, 2036 (1982); P. J. Kavinsky, N. B. Madsen, J. Syguch, R. J. Fletterick, *J. Biol. Chem.* **253**, 3343 (1978); P. J. Kavinsky, S. Schechosky, R. J. Fletterick, *ibid.*, p. 9102.
18. C. Chothia, M. Levitt, D. Richardson, *Proc. Natl. Sci. Acad. U.S.A.* **74**, 4130 (1977).
19. W. S. Bennett and T. A. Steitz, *J. Mol. Biol.* **140**, 211 (1980); S. Remington, G. Wiegand, R. Huber, *ibid.* **158**, 111 (1982); J. F. Krisch, G. Eichele, G. C. Ford, M. G. Vincent, J. N. Jansonius, *ibid.* **174**, 494 (1984).
20. K. L. Krause, K. W. Volz, W. N. Lipscomb, *ibid.* **193**, 527 (1987); P. R. Evans, G. W. Farrants, M. C. Lawrence, *ibid.* **191**, 713 (1986).
21. W. A. Hendrickson, *Acta Cryst.* **A34**, 931 (1979).
22. Supported by NIH grants GM00085-05 (R.J.F.) and DK31507-05 (S.R.S.). We thank N. Madsen and S. Schechosky for providing the parent crystals and A. Strand for assistance with TNT refinement. Atomic coordinates to be deposited in the Brookhaven Protein Data Bank.

9 January 1989; accepted 28 April 1989

5-Bromo-2′-Deoxyuridine Blocks Myogenesis by Extinguishing Expression of MyoD1

STEPHEN J. TAPSCOTT, ANDREW B. LASSAR, ROBERT L. DAVIS, HAROLD WEINTRAUB

The pyrimidine analog 5-bromodeoxyuridine (BUdR) competes with thymidine for incorporation into DNA. Substitution of BUdR for thymidine does not significantly affect cell viability but does block cell differentiation in many different lineages. BUdR substitution in a mouse myoblast line blocked myogenic differentiation and extinguished the expression of the myogenic determination gene MyoD1. Forced expression of MyoD1 from a transfected expression vector in a BUdR-substituted myoblast overcame the block to differentiation imposed by BUdR. Activation of BUdR-substituted muscle structural genes and apparently normal differentiation were observed in transfected myoblasts. This shows that BUdR blocks myogenesis at the level of a myogenic regulatory gene, possibly MyoD1, not by directly inhibiting the activation of muscle structural genes. It is consistent with the idea that BUdR selectively blocks a class of regulatory genes, each member of which is important for the development of a different cell lineage.

THE SUBSTITUTION OF BUDR FOR thymidine in DNA has the effect of blocking the expression of the differentiated phenotype in many different cell lineages without significantly altering the general, or household, functions of a cell or cell viability (*1–4*). The ability of BUdR to block differentiation is directly related to the degree of DNA substitution, and, in general, the effect is reversible when cells are cultured in the absence of BUdR and the analog is replaced by thymidine during DNA replication (*5*). Therefore, BUdR is not acting as a mutagen, but is reversibly blocking the differentiation program of a wide variety of cell types in a manner dependent on BUdR incorporation into DNA (*6, 7*).

Although the mechanism by which BUdR blocks differentiation is not known, two types of experiments have suggested that BUdR inhibits differentiation by influencing a small number of regulatory loci: (i) During chick erythropoiesis, increasing concentrations of BUdR result in the production of progressively fewer erythrocytes; however, the erythrocytes that are formed, even at high levels of BUdR substitution, are normal in every way tested (*3*). This all-or-none effect of BUdR inhibition, together with the observation that the dose-response curve was consistent with only a few targets per cell (*8*), suggested that the primary effect of BUdR is the inactivation of a regulatory gene, or master switch, for erythropoiesis (*9*). (ii) In primary chick myoblast cultures blocked from differentiation by a single round of DNA replication in BUdR, the kinetics of myotube differentiation after removal of BUdR and resubstitution with thymidine suggested that the BUdR-sensitive target or targets segregated with only one pair of chromosomes (*10*).

Recently, we have identified a nuclear protein, MyoD1, which can activate the myogenic program in many, but not all, cell types (*11*). The cDNA for this protein was isolated by subtractive hybridization of cDNA from a myoblast line derived from

S. J. Tapscott, Department of Genetics, Fred Hutchinson Cancer Research Center, 1124 Columbia Street, Seattle, WA 98104, and Division of Neurology, University of Washington, Seattle, WA 98195.
A. B. Lassar, Department of Genetics, Fred Hutchinson Cancer Research Center, Seattle, WA 98104.
R. L. Davis, Department of Genetics, Fred Hutchinson Cancer Research Center, Seattle, WA 98104 and Department of Pathology, University of Washington, Seattle, WA 98195.
H. Weintraub, Department of Genetics, Fred Hutchinson Cancer Research Center, Seattle, WA 98104 and Department of Zoology, University of Washington, Seattle, WA 98195.